scientific reports

Check for updates

OPEN

Irradiated umbilical cord mesenchymal stem cell-coated high oxygen-permeable hydrogel lenses inhibit corneal inflammation and neovascularization after corneal alkali burns

Siqi Song[1,3], Yaqi Cheng[1,3], Weihua Li[2], Huan Yu[2], Zhiquan Li[2], Jianbing Li[1], Meng Li[1], Qunai Huang[1], Yingjie Liu[1] & Shiqi Ling[1]✉

Corneal alkali burns can cause persistent inflammation and corneal neovascularization. In this study, we divided corneal alkali burned rabbits into the untreated group, the blank lens group, the radiation-treated umbilical cord mesenchymal stem cells (UCMSC) lens group, and the UCMSC I.V. group, and then measured corneal inflammation, neovascularization and corneal injury repair via slit lamp microscopy, captured anterior segment optical coherence tomography (AS-OCT), and performed hematoxylin-eosin staining. Compared with those in the other experimental groups, radiation-treated UCMSC lenses significantly decreased inflammatory index (IF) scores, areas of corneal blood vessels and corneal epithelial injury. The expression of interleukin (IL)-17 in corneas treated with radiation-treated UCMSC lenses was lower than that in corneas treated with blank lenses, and radiation-treated UCMSC lenses exhibited greater expression of IL-4 and signal transducer and activator of transcription 1 (STAT1), while the expression of cluster of differentiation-3G (CD3G), a linker for the activation of T cells (LAT), IL-6, IL-1B, CC chemokine receptor 6 (CCR6) and IL-23 exhibited the opposite effects (all $P < 0.05$). Our findings demonstrated that irradiated UCMSC-coated high oxygen-permeable hydrogel lenses on the ocular surface inhibited corneal angiogenesis and inflammation after corneal alkaline burns. The downregulation of Th17 cell differentiation might be responsible for these effects.

Keywords Radiation-treated umbilical cord stem cells, Alkali corneal burns, Inflammation, Angiogenesis, Th17 cell differentiation

An alkali corneal burn is a severe injury that can result in permanent blindness[1]. Following an alkali burn, inflammatory cells such as leukocytes rapidly release proteolytic enzymes and inflammatory mediators, which promote the degradation of ocular structures[2]. This process initiates a chain reaction in which the damaged tissues secrete proteases, causing further damage and leading to a vicious cycle of degradation. Persistent corneal epithelial defects and corneal ulcers are the main characteristics after alkali burns[3], and corneal neovascularization, limbal stem cell deficiency and corneal opacity may also occur after corneal injury repair[4]. These complications can be severe, requiring surgeries such as lamellar/penetrating keratoplasty and limbal tissue grafts[5–7]. However, these surgeries cannot meet increasing clinical needs because of the lack of donors[8]. In addition, rejection after corneal transplantation may lead to surgical failure, so it is necessary to use hormone drugs and immunosuppressants locally to avoid it, which may lead to opportunistic infections[6]. The use of hormone drugs may also lead to glaucoma, cataracts and other eye diseases[9].

[1]Department of Ophthalmology, The Third Affiliated Hospital, Sun Yat-Sen University, Guangzhou, P.R. China. [2]State Key Laboratory of Ophthalmology, Zhongshan Ophthalmic Center, Guangdong Provincial Key Laboratory of Ophthalmology and Visual Science, Sun Yat-sen University, Guangzhou 510060, China. [3]Siqi Song and Yaqi Cheng contributed equally to this work. ✉email: lingshiqi123@163.com

Mesenchymal stem cells (MSCs), which are derived from adult stem cells in the mesoderm, can differentiate into various tissues, such as bone and muscle[10]. MSCs have recently been used to treat alkali corneal burns due to their wide range of physiological effects, such as their anti-inflammatory and repair abilities, which have shown promising results[11–15]. Different methods have been used to deliver MSCs, including eye drops[12], exosomes[13,14], transplantation via amniotic membranes[15] and intraperitoneal (I.P.)[12], intravenous (I.V.)[12], and subconjunctival injections[11]. MSCs injected via the I.P. or I.V. route have been used to treat animal ocular surface diseases[16]. However, they are invasive treatment methods, and the potential tumorigenicity of such injected stem cells that reach the target organ and function through the circulation of blood seriously restricts their clinical use[17,18]. In previous research, MSC radiation has been used to inhibit MSC proliferation and tumorigenicity[19]. Although ocular local drug delivery methods can selectively deliver drugs to the anterior segment of the eyes, the small volume of the conjunctival sac limits drug capacity[20], and precorneal fluid drainage, including nasolacrimal duct drainage, causes a short residence time of drugs on the corneal surface[21], which greatly limits the utilization rate of MSCs and the effectiveness of this method. Exosomes are a cell-free drug delivery method that can avoid the tumorigenicity and tumorigenicity of MSCs, but it is difficult to meet the actual clinical needs due to the short half-life of their local use, difficult extraction and identification, and high preservation requirements[22]. The method of generating MSCs with amniotic membranes needs to be realized by surgery, and the amniotic membrane usually dissolves approximately 2 weeks after surgery, which forces us to perform the operation again to provide attachment for MSCs, which limits their clinical application[23]. In summary, we need to find a suitable way to utilize MSCs efficiently and safely.

We constructed drug-based combination lenses composed of silicone hydrogel lenses and radiation-treated umbilical cord MSCs (UCMSCs) to sustainably produce immunomodulatory cytokines in the conjunctival sac and avoid the side effects of UCMSCs. In recent researches, we demonstrated that these lenses could effectively maintain activity and immune function and treat graft-versus-host disease successfully[24]. However, there are few reports on the successful local use of UCMSCs, and the mechanism by which UCMSCs inhibit corneal alkali burn after irradiation is poorly understood. Therefore, the objective of this study was to investigate whether irradiated umbilical cord mesenchymal stem cell-coated high oxygen-permeable hydrogel lenses (radiation-treated UCMSC lenses) exert therapeutic effects on corneal alkali burns and to explore the underlying mechanisms involved.

Results

Radiation-treated UCMSCs maintained viability on lenses

Radiation-treated umbilical cord mesenchymal stem cells UCMSCs cultured on lenses demonstrated high viability after 1 day at room temperature, with a cell viability of $(97.7 \pm 0.58)\%$ and a cell count of $(1.49 \pm 0.12) \times 10^5$. Although both the cell number and survival rate exhibited a gradual decline over time, the UCMSCs on the lenses retained significant viability throughout the culture period. By day 5, the live cell count was $(1.14 \pm 0.06) \times 10^5$, and the viability rate remained high at $(87 \pm 6.56)\%$. These results indicate that the majority of UCMSCs can maintain their activity on the lenses for at least 5 days under the tested conditions.

Radiation-treated UCMSC lenses reduced corneal inflammation

To assess the degree of corneal inflammation, we utilized a slit lamp, which has been widely used to assess inflammation severity in the cornea, to record Inflammatory index (IF) scores on days 3, 7, 10, 14, and 18 (Fig. 1A-C)[24–28]. Compared with the IF scores of the normal corneas (Fig. 1B), the IF scores of the other groups gradually increased with time after the burn and peaked on day 18, except for the blank lens group, which had the highest scores on day 14, and the scores of the radiation-treated UCMSC lens group were consistently lower than those of the other groups on days 7, 10, 14 and 18 after corneal alkali burn injury ($P < 0.05$) (Fig. 1C). The rabbits in the radiation-treated UCMSC lens group exhibited mild to moderate ciliary congestion, with congested vascular lengths usually between 1 and 2 mm. In most of the rabbits treated with the radiation-treated UCMSC lenses, the pupils and peripheral iris were visible at 18 days after the burn, indicating mild corneal inflammation.

To further examine corneal inflammation, central corneal thickness was assessed using anterior segment optical coherence tomography (AS-OCT) after corneal alkali burns (Fig. 2A). By measuring central corneal thickness, the degree of central corneal edema can be determined, providing a tool to evaluate inflammation status. The results demonstrated that the central corneal thickness of the four experimental groups peaked on day 3 and decreased in all groups over time. Among the groups, the resolution of edema was faster in the radiation-treated UCMSC lens group, and on day 18, the thickness had almost returned to that before the alkali burn (Fig. 2B).

After HE staining, we found that the corneas of the untreated group and the blank lens group were significantly thicker than those of the other groups (Fig. 2C,D). In the blank lens group, all layers of corneal tissue were seriously edematous, while in the untreated group, corneal tissue was significantly damaged, with new blood vessels and a large amount of fibrous tissue hyperplasia, many inflammatory cells infiltrated, and corneal stromal cells were significantly more disordered than normal corneal stromal cells. In contrast, the degrees of tissue inflammation, corneal edema and corneal stroma destruction in the radiation-treated UCMSC lens group and the UCMSC I.V. group treated with UCMSCs were less than those in the other two groups, which indicates that radiation-treated UCMSC lenses have better therapeutic effects than blank lenses.

Based on slit-lamp examination, AS-OCT, and HE staining, we concluded that radiation-treated UCMSC lenses significantly reduce corneal inflammation following corneal alkali burns.

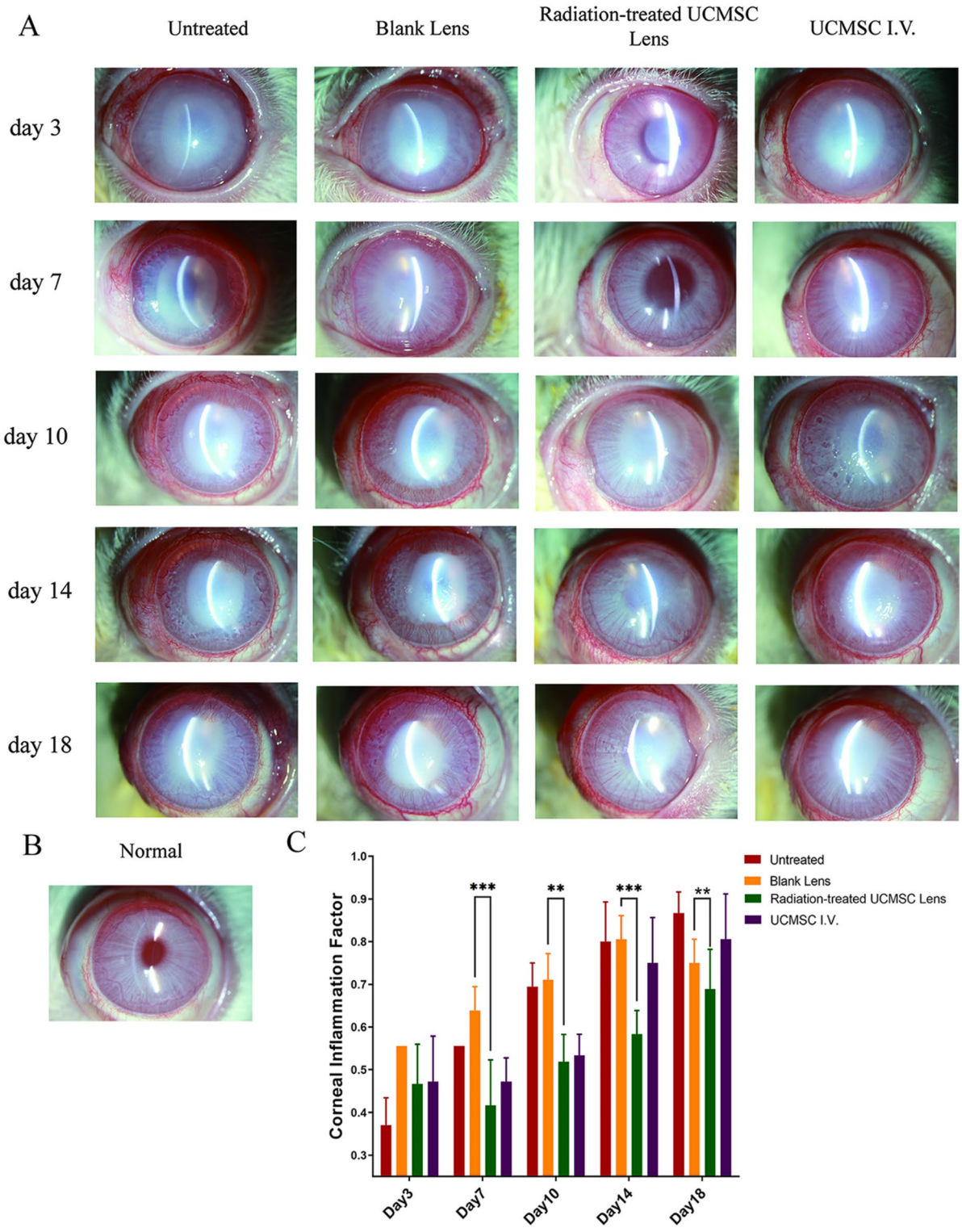

Fig. 1. The slit lamp cornea imaging results and the related inflammatory index findings. Slit-lamp images of rabbit corneas from the different experimental groups are shown for 3, 7, 10, 14, and 18 days (as demonstrated in (**A**)). A representative slit lamp image of a normal rabbit cornea is displayed in (**B**). A bar graph of inflammatory indexes over time (on days 3, 7, 10, 14, and 18) is shown in (**C**). The statistical analysis indicated significant differences at $^{*}P<0.05$, $^{**}P<0.01$, and $^{***}P<0.001$.

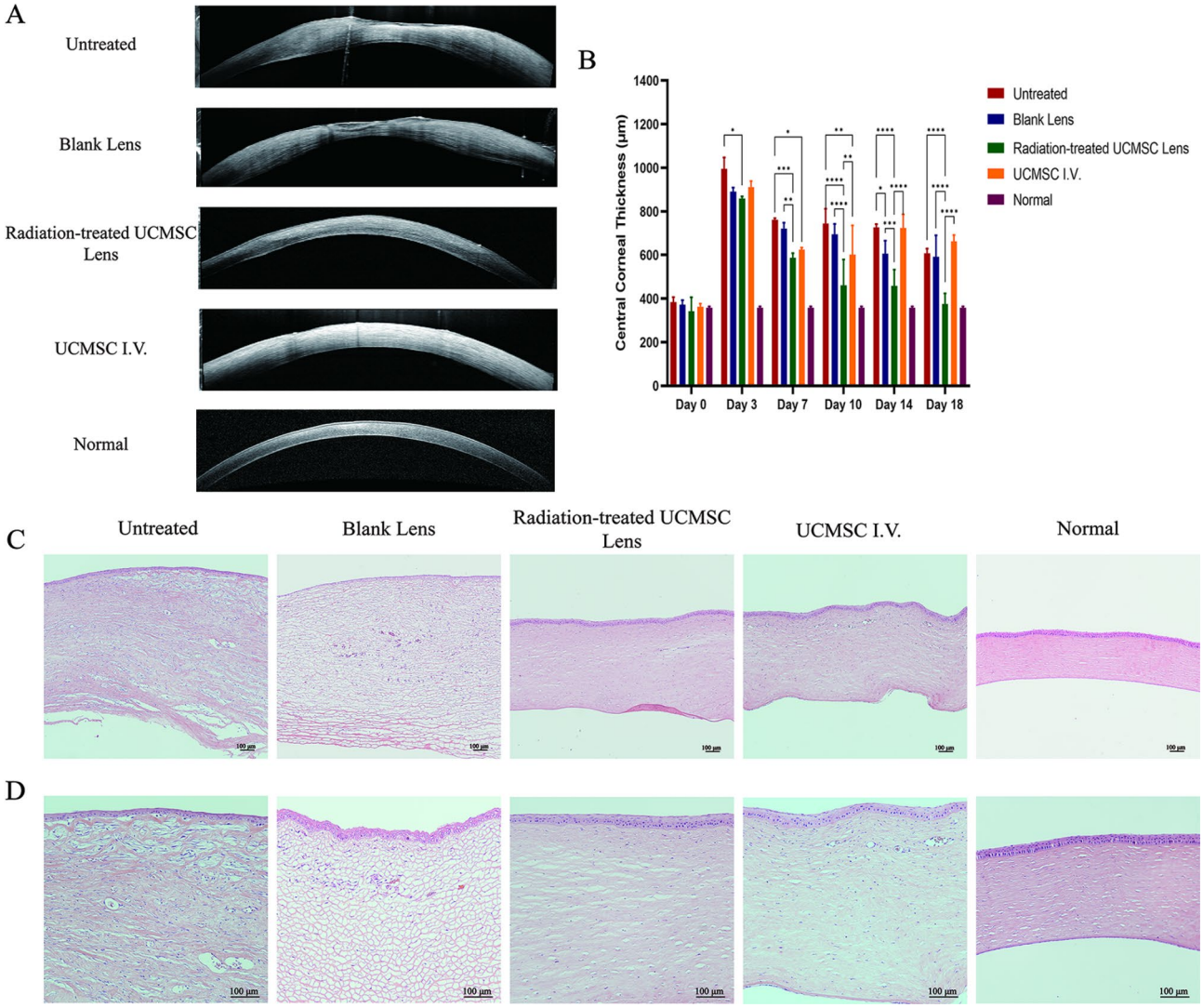

Fig. 2. Images of AS-OCT images and HE-stained corneas in each group on day 18. AS-OCT imaging revealed that the normal corneal surfaces were smooth and that the corneal stroma was generally homogeneous. In contrast, the corneas in the other groups displayed varying degrees of edema or ulceration. Among these groups, the radiation-treated UCMSC lenses effectively reduced corneal edema and prevented ulcer formation (as depicted in (**A**)). A bar plot of the central corneal thickness is shown in (**B**). Images of corneal HE-stained tissues from the various groups under a light microscope showed that the inflammation of the corneal tissue in the blank lens group and the untreated group was more severe than that in the other groups ((**C**): magnification×100; (**D**): magnification×200). The statistical analysis indicated significant differences at $^{*}P<0.05$, $^{**}P<0.01$, $^{***}P<0.001$, and $^{****}P<0.0001$.

Radiation-treated UCMSC lenses inhibited corneal angiogenesis

We also found that corneal neovascularization was inhibited by radiation-treated UCMSC lenses. Corneal angiogenesis, occurring at 3 days, gradually developed and peaked at 18 days after the burn, and the angiogenesis progressed from the limbus to the center of the cornea, similar to a hair brush (Fig. 3A). However, among the four experimental groups, the area of corneal angiogenesis in the radiation-treated UCMSC lens group was significantly lower than that in the other three experimental groups on days 10, 14, and 18 (all $P<0.05$; Fig. 3B). On day 18 after alkali burn injury, corneal angiogenesis was greatest in the blank lens group and the untreated group, with mean areas of corneal neovascularization of 118 mm^2 and 113 mm^2, respectively, followed by the UCMSC I.V. group (65 mm^2) and the radiation-treated UCMSC lens group (45 mm^2).

To elucidate the mechanisms through which radiation-treated UCMSC lenses inhibit neovascularization, we examined the expression levels of vascular endothelial growth factor (VEGF), matrix metalloproteinase 1 (MMP1), MMP2, and MMP9. VEGF is a well-characterized angiogenic factor that plays a critical role in promoting the proliferation and migration of endothelial cells (ECs)[29]. Similarly, MMP1, MMP2, and MMP9 are critical enzymes involved in extracellular matrix (ECM) degradation, angiogenesis, and inflammatory responses. Their upregulation is closely associated with corneal neovascularization, as they facilitate endothelial

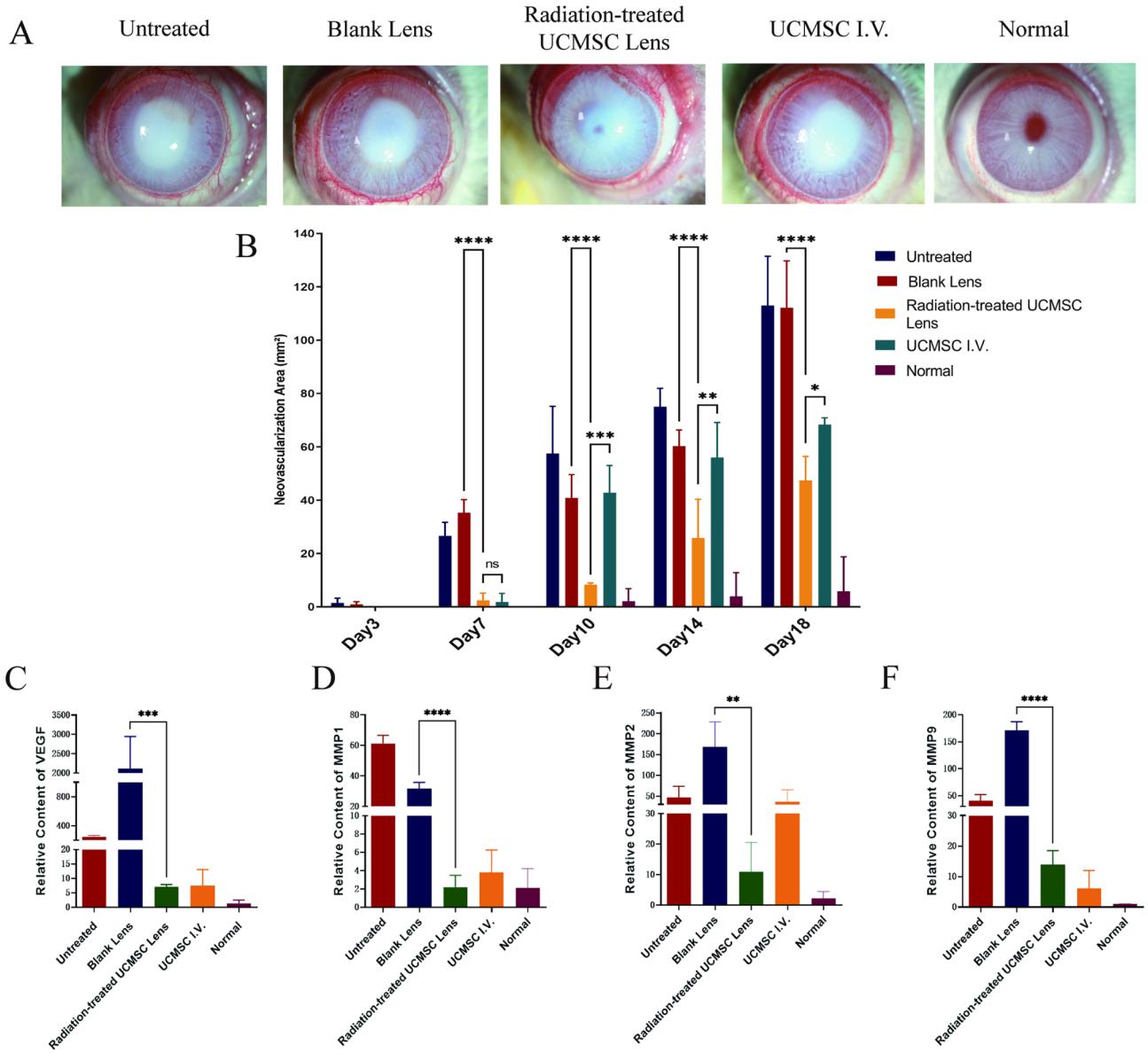

Fig. 3. Corneal angiogenesis and inflammatory factor levels were significantly reduced after treatment with radiation-treated UCMSC lenses (**A**). The data are presented as representative images and a bar plot (**B**) of the neovascularization areas, demonstrating statistical significance (*$P<0.05$; **$P<0.01$; ***$P<0.001$; ****$P<0.0001$). To assess inflammatory cytokines, PCR analysis was conducted (**C**-**F**), and the mRNA levels of VEGF, MMP-1, MMP-2, and MMP-9 were analyzed on day 18. Statistical significance is represented as follows: *$P<0.05$; **$P<0.01$; ***$P<0.001$; ****$P<0.0001$.

cell migration and vessel formation by remodeling the ECM[30,31]. Our results suggested that radiation-treated UCMSC lenses reduced corneal neovascularization by releasing growth factors. After 18 days of treatment, vascular endothelial growth factor (VEGF) expression was the highest in the blank lens group, followed by the untreated group. The UCMSC I.V. group exhibited lower VEGF expression, with the lowest expression observed in the radiation-treated UCMSC lens group. VEGF expression in the blank lens group was 6.9 times greater than that in the radiation-treated UCMSC lens group, while it was 5.2 times greater in the untreated group than in the UCMSC I.V. group (Fig. 3C). Matrix metalloproteinase 1 (MMP1), MMP2, and MMP9 expression was generally lower in the radiation-treated UCMSC lens group and the UCMSC I.V. group (Fig. 3D-F). The downregulation of these MMPs in the UCMSC groups suggests a suppression of ECM degradation and angiogenesis, thereby inhibiting the neovascularization process.

Based on the findings above, it is concluded that radiation-treated UCMSC lenses significantly inhibit corneal neovascularization following alkali burns.

Radiation-treated UCMSC lenses promoted corneal recovery

In this study, the fluorescence staining area suggested damage from the alkali burn, and a change in its size indicated repair or deterioration of the cornea. On the 18th day after corneal alkali burn, corneal epithelial defects of different degrees were still observed in all groups (Fig. 4A). Although the area of corneal epithelial injury in the radiation-treated UCMSC lens group was smaller than that in the other groups except on day 7 (Fig. 4B), there was no statistically significant difference among the groups on days 3, 7, 10 and 14 after corneal alkali burn ($P > 0.05$). However, on the 18th day, the rate of corneal epithelial injury in the radiation-treated UCMSC lens group was significantly lower than that in the other groups (all $P < 0.05$), except for the UCMSC I.V. group ($P > 0.05$) (Fig. 4C). These findings suggest that UCMSCs play a significant role in corneal wound healing 18 days post-alkali burn.

Transcriptome sequencing indicated that radiation-treated UCMSCs suppressed the T helper 17 (Th17) cell differentiation pathway in alkali corneas

To identify key genes and pathways associated with the therapeutic effects of radiation-treated UCMSC lenses on alkali corneal burns, we profiled the transcriptomes of corneas from the blank lens group and the radiation-treated UCMSC lens group on day 18 by transcriptome sequencing and performed a differential gene expression analysis. A heatmap of the top 100 upregulated and downregulated DEGs is shown, and relative consistency was observed between the groups (Fig. 5A). We found extensive changes in gene expression between the blank lens group and the radiation-treated UCMSC lens group, with 378 genes upregulated (>2-fold; $p < 0.05$) and 228 downregulated (>2-fold; $p < 0.05$, Fig. 5B) in group C. KEGG and GSEA analyses of the RNA-seq dataset (Fig. 5C) revealed that the downregulated DEGs were significantly enriched in the Th17 cell differentiation pathway.

Irradiated UCMSCs inhibited the growth of Th17 cells

Th17 cells are a newly discovered $CD4^+$ T-cell subset characterized by the production of Interleukin 17 (IL-17)[32]. The results of flow cytometry analysis after the coculture of peripheral blood mononuclear cells (PBMC) with irradiated UCMSCs are shown in Fig. 6. The proportions of Th17 cells among the PBMCs in the low-density

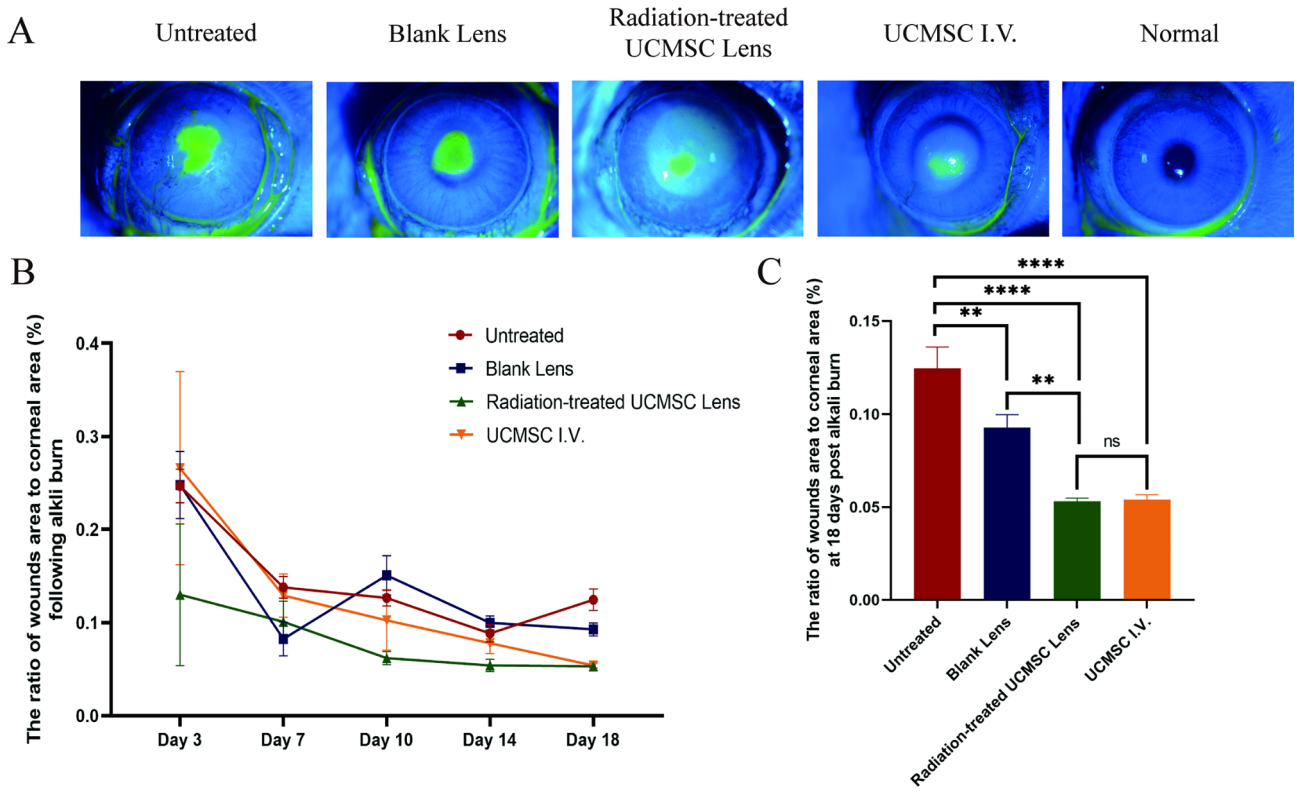

Fig. 4. The anterior segment of the eyes on the 18th day after alkali burn under cobalt blue light and the curve and the 18th day's histogram of the corneal epithelial injury rate. After corneal fluorescence staining was performed on the 18th day, we found that the stained area in the radiation-treated lens group was smaller than that in the other groups (**A**). The change curve of the corneal epithelial injury rate in each group is shown in figure (**B**), and the corneal epithelial injury rate of the radiation-treated UCMSC lens group was the lowest on the 18th day compared with that of the other groups (**C**) ($P < 0.05$). There were significant differences according to the statistical analysis results: (ns: no significance; $^*P < 0.05$, $^{**}P < 0.01$, $^{***}P < 0.001$, $^{****}P < 0.0001$. The error bars in the chart represent the standard deviation.

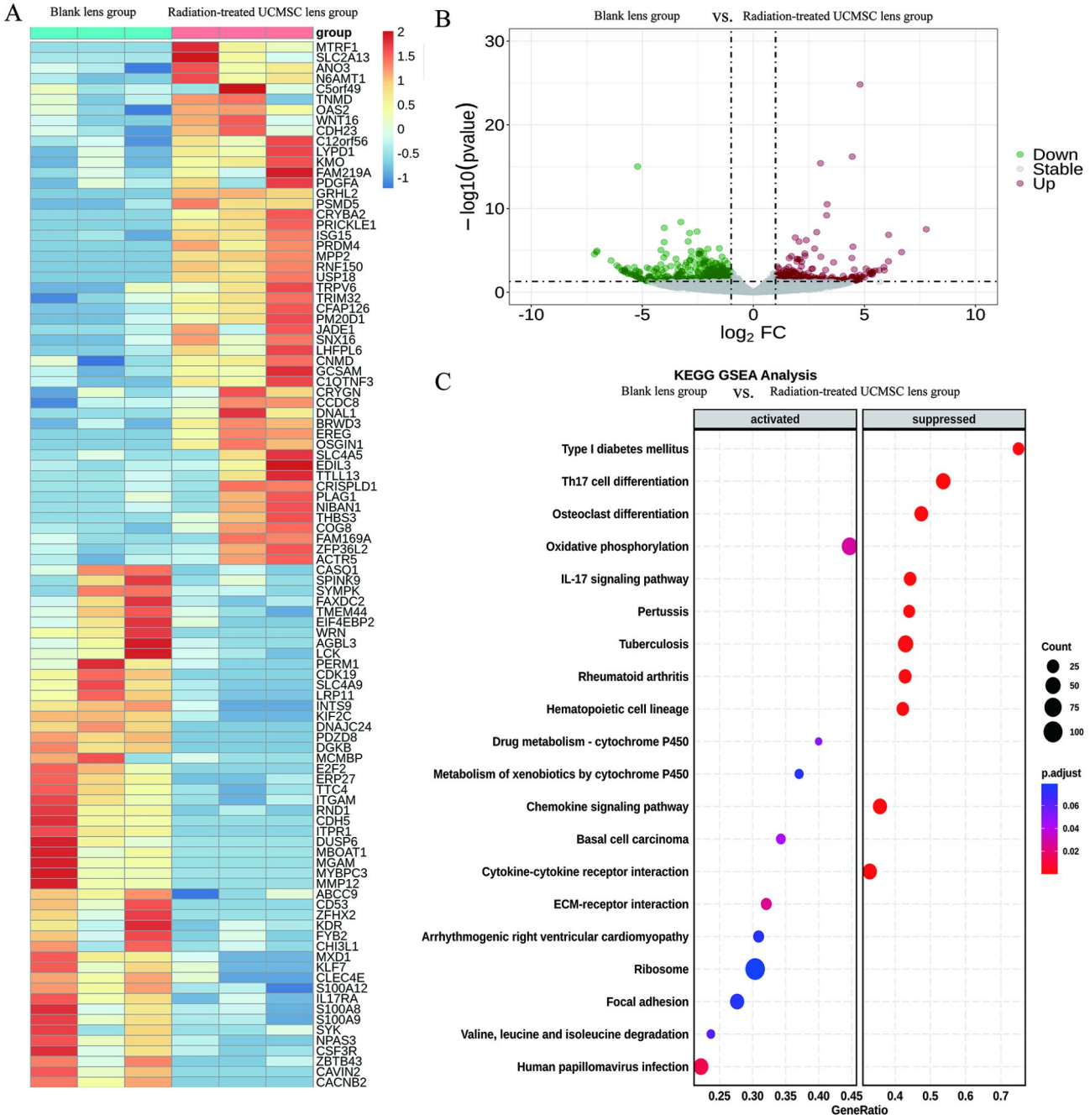

Fig. 5. Inflammatory pathways involved in the treatment of corneal alkali burn injury by radiation-treated UCMSC lenses. (**A**) Heatmap of DEGs in the blank lens group vs. the radiation-treated UCMSC lens group. (**B**) The volcano plot shows the number and magnitude of DEGs in the blank lens group vs. the radiation-treated UCMSC lens group. The plot indicates the -log 10 p value for genome-wide genes (Y-axis) plotted against their respective log 2-fold change (X-axis). The red and green dots represent significantly up- and downregulated genes, respectively, in the blank lens group (fold change > 2, p value < 0.05), and the opposite results were observed in the radiation-treated UCMSC lens group. (**C**) A dot plot showing the biological pathways that are enriched during alkali corneal burn injury according to gene set enrichment analysis (GSEA). The ordinate indicates the pathway (sorted by gene ratio value), and the abscissa indicates the ratio of the number of DEGs annotated to the pathway to the total number of DEGs. The size of the points represents the number of genes annotated to the pathways, and the color represents the significance. In the top picture, "activated" means upregulated in the radiation-treated UCMSC lens group, and "suppressed" means downregulated in the radiation-treated UCMSC lens group.

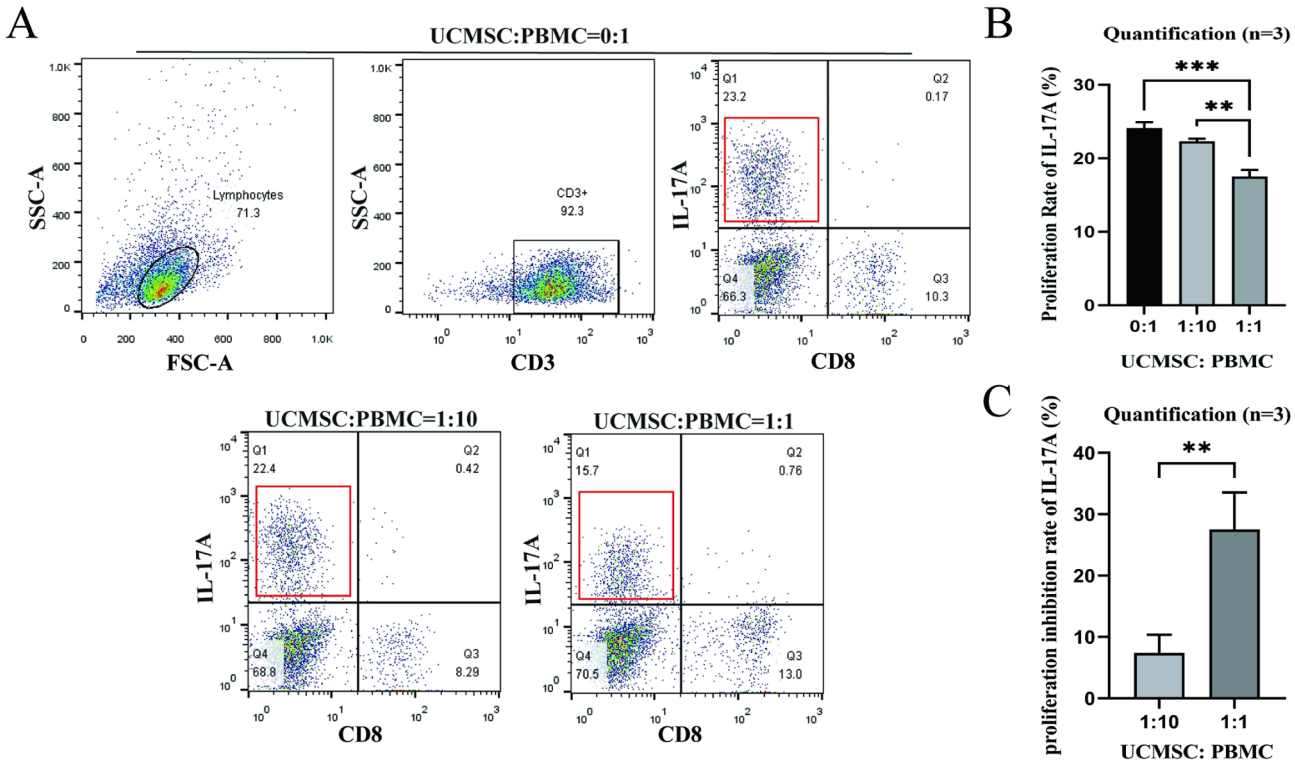

Fig. 6. Flow cytometry was performed to analyze the surface markers present on Th17 cells, and the results indicated the presence of CD3(+), IL-17 A(+) and CD8 (-) on Th17 cells (**A**). The authors showed that irradiated UCMSCs can decrease the proportion of Th17 cells among PBMCs (**B**). Additionally, compared to low-concentration UCMSCs (UCMSC: PBMC ratio of 1:10), high-concentration UCMSCs (UCMSC: PBMC ratio of 1:1) exhibited a significantly stronger inhibitory effect on IL-17 proliferation. The difference in proliferation inhibition rates between the two groups was statistically significant (**C**). Statistical analysis revealed significant differences, with $^{**}P<0.01$, $^{***}P<0.001$. The error bars in the charts represent the standard deviation.

group and high-density group were 22.31% and 17.50%, respectively, and the corresponding inhibition rates were 7.43% and 27.66%, respectively.

Immunohistochemistry, enzyme-linked immunosorbent assay (ELISA) and quantitative reverse transcription-polymerase chain reaction (qRT–PCR) results showing that irradiated UCMSCs effectively treat alkali burns by downregulating the Th17 cell differentiation pathway

Th17 cell differentiation can be initiated by transforming growth factor-β (TGF-β) together with the inflammatory cytokines IL-1β, IL-6, and IL-23[33]. IL-2, IL-4, IL-27 and interferon-γ (IFN-γ) can abrogate Th17 differentiation through signal transducer and activator of transcription 5 (STAT5), STAT6 and STAT1 activation, respectively[34]. In humans, IL-23 or IL-1 induces the differentiation of Th17 cells that express IL23R and CC chemokine receptor 6 (CCR6)[12,35]. In addition, recent studies have reported that the linker for the activation of T-cell (LAT)-related signals and CD3G are closely related to the Th17 cell differentiation pathway[36,37].

To determine whether radiation-treated UCMSC lenses can effectively treat alkali corneal burns by downregulating the Th17 cell differentiation pathway, immunohistochemistry, ELISA and qRT-PCR were performed. With immunohistochemical staining, IL-17-positive cells were stained brown, and we observed many IL-17-positive cells in corneas from the blank lens group (Fig. 7A_1, A_2) but few in those from the radiation-treated UCMSC lens group (Fig. 7B_1, B_2). The ELISA results showed that the level of IL-17 in the isolated corneas of the rabbits in the radiation-treated UCMSC lens group was lower than that in the isolated corneas of the rabbits in the blank lens group ($P<0.05$, Fig. 7C).

In addition, PCR (Fig. 7D) showed that the expression levels of IL-17 A, CD3G, LAT, IL-1B, IL-6, CCR6 and IL-23 in the blank lens group were significantly greater than those in the radiation-treated UCMSC lens group ($P<0.05$), and the expression level of IFN-γ in the radiation-treated UCMSC lens group was greater than that in the blank lens group, but the difference was not statistically significant ($P>0.05$). The expression levels of IL-4 and STAT1 in the radiation-treated UCMSC lens group were greater than those in the blank lens group ($P<0.05$). These results further demonstrate that UCMSCs-laden lenses downregulate the Th17 cell differentiation pathway.

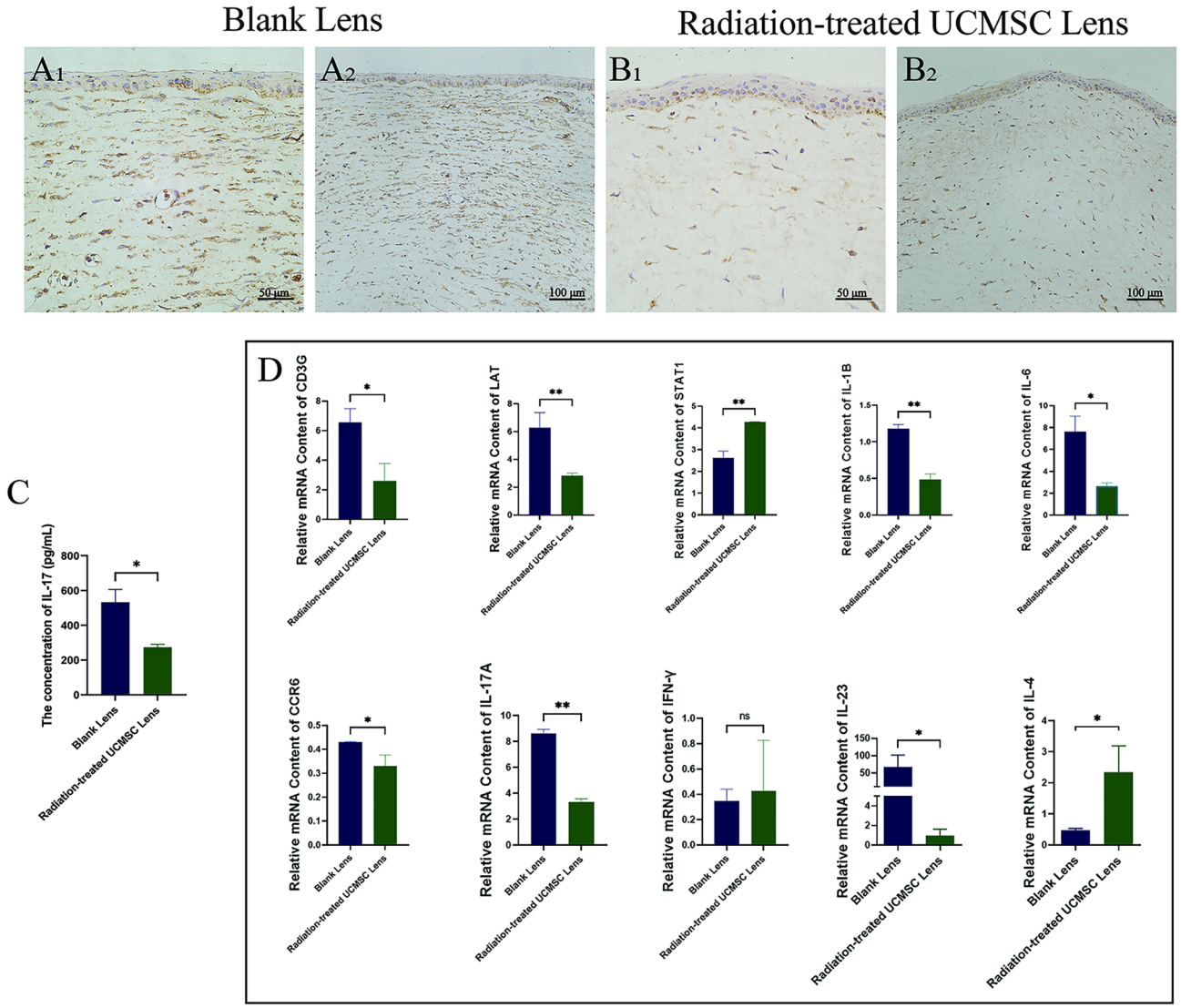

Fig. 7. Immunohistochemistry, ELISA and PCR analysis of IL-17 in injured rabbit corneas. Compared with that in the corneas of the left eye, the expression of the IL-17 protein in the blank lens group was dramatically greater, and the IL-17-positive cells were mainly concentrated in the corneal stroma ($\mathbf{A}_1$,$\mathbf{B}_1$), magnification×400; ($\mathbf{A}_2$,$\mathbf{B}_2$), magnification×200.). The concentrations of IL-17 (**C**) and the mRNA (**D**) levels of CD3G, LAT, STAT1, IL-1B, IL-6, CCR6, IL-17 A, IFN-γ, IL-23, and IL-4 in the blank lens group and the radiation-treated UCMSC lens group were analyzed on day 18. A t test was carried out to compare the differences between the blank lens group and the radiation-treated UCMSC lens group. The statistical significance is represented as follows: $^{*}P<0.05$; $^{**}P<0.01$; $^{***}P<0.001$; $^{****}P<0.0001$.

Discussion

In this study, radiation-treated UCMSC lenses were prepared by combining highly oxygen-permeable hydrogel lenses with irradiated UCMSCs, forming a novel therapeutic modality that could utilize immune modulation by UCMSCs to reduce corneal inflammation and neovascularization.

MSCs are adult mesenchymal stem cells with immunoregulatory functions that have been used to treat corneal alkali burns in some studies and have achieved good curative effects[38–40]. However, intravenous use of UCMSCs has the potential risk of stimulating tumor growth through intercellular interactions to stimulate the development of ovarian tumors[41] and can also enhance the proliferation and migration of cancer cells[42,43]. In addition, human leukocyte antigen (HLA)-mismatched MSCs are eliminated by the host immune system[44]. Moreover, it has been reported that less than 1% of systemic infusions of MSCs reach the target tissue[45,46]. Most systemically used MSCs are trapped in the lungs, thus affecting their immune activity[47,48]; therefore, many cells are usually required to achieve the desired therapeutic effect, which limits the feasibility of applying mesenchymal stem cell-based therapies in the clinic[45].

Therefore, the benefit of using MSCs locally to treat corneal alkali burns is that the drug acts directly on the target organ, theoretically preventing MSCs from entering the systemic circulation and bypassing the lung first-pass effect to target delivery cells[49] to improve drug utilization efficiency.

However, keeping UCMSCs on the surface of the eye without the help of other drugs is difficult. Currently, the principal preservation method for UCMSCs is to use Matrigel to support the growth of UCMSCs[50,51], but Matrigel is not a scientifically approved product, so it is impossible to use clinically. In previous studies, several researchers have identified MSCs. They were attached to fibrin gel and then transplanted into the cornea[52], while other researchers used MSCs implanted into amniotic membranes[15,53]. However, fibrin has previously been reported to alter the phenotypic and functional characteristics of stem cells[54]. In addition, the amniotic membrane has inherent immunosuppressive potential[27,55], which affects its therapeutic efficacy.

To safely and efficiently apply UCMSCs to the ocular surface, we developed a radiation-treated UCMSC lens (China invention patent: ZL202011504302.4) composed of irradiated UCMSCs and specific silicone hydrogel lenses to provide both a sustainable immunomodulatory effect and high oxygen permeability. In our previous study, the authors retained most of the irradiated UCMSCs (15 Gy) on silicone hydrogel lenses for at least 5 days and maintained their immunomodulatory effects, which helped these lenses treat corneal alkali burns. The results also indicated that a high dose of UCMSCs (2.0×10^5 cells) on lenses had the greatest effect on both anti-inflammatory and antineovascularization effects in the treatment of corneal alkali burns[24].

After establishing the rabbit alkali burn model, the groups were established as follows. First, the radiation-treated UCMSC lenses were composed mainly of blank hydrogel lenses and irradiated UCMSCs. Interference of lenses on therapeutic effect should be excluded. Therefore, the efficacy of UCMSCs on radiation-treated UCMSC lenses should be compared between the blank lens group and the radiation-treated UCMSC lens group. Second, the use of radiation-treated UCMSC lenses is characterized by the local use of UCMSCs, and the UCMSC I.V. group was established to explore whether local application can obtain better results than systematic use of UCMSCs. Third, comparisons were made between the untreated group and the UCMSC I.V. group to observe the therapeutic effect of UCMSCs. Fourth, a blank normal group was used to determine the indicators of a normal cornea to assess abnormalities after corneal alkali burn and recovery in the treatment group. Overall, we established four experimental groups and one normal control group.

Compared with those in the blank lens group and the radiation-treated UCMSC lens group, the IF value, degree of corneal edema, neovascular area and degree of corneal epithelial damage in the latter group were significantly lower, which indicates that the local use of UCMSCs is effective for anti-inflammatory and corneal repair. In addition, the PCR results demonstrated that the local use of UCMSCs can reduce neovascularization by downregulating vascular growth-related factors.

Compared with the untreated group and the UCMSC I.V. group, the systemic use of UCMSCs had a certain therapeutic effect on the treatment of corneal alkali burns by reducing neovascularization and inflammation and promoting corneal repair.

The results from the two groups above showed that both systemic and local use of UCMSCs inhibited inflammation and neovascularization after alkali burn injury and promoted corneal repair.

Finally, the therapeutic effects of intravenous injection of UCMSCs and radiation-treated UCMSC lenses after corneal alkali burn injury were compared, and the results showed that there was less inflammation and corneal neovascularization in the radiation-treated UCMSC lens group than in the UCMSC I.V. group. The above results suggested that the local use of UCMSCs in radiation-treated UCMSC lenses was more effective than the systemic use of UCMSCs in the treatment of inflammation and neovascularization ($P < 0.05$). However, there was no significant difference in the extent of corneal epithelial injury repair ($P > 0.05$). In conclusion, the efficacy of radiation-treated UCMSCs is significantly better than that of systemic UCMSCs, especially in terms of their anti-inflammatory and antivascular effects.

To determine how radiation-treated UCMSC lenses function when they cover the surface of injured eyes, we performed GSEA and KEGG analyses between the blank lens group and radiation-treated UCMSC lens group, considering that the effects of the treatment were influenced by many factors, including UCMSCs, blank lenses, alkali burn, and intravenous injection, which rigorously excluded these influencing factors.

Our results showed that radiation-treated UCMSC lenses play a role in treating alkali corneal burns via Th17 cell differentiation and the successful regulation of relevant cytokines.

First, in the GSEA and KEGG analyses, Th17 cell differentiation was the second most enriched pathway. The top-ranked enriched pathway, the pathway of type I diabetes mellitus, is closely related to endocrine disease, a disorder of carbohydrate metabolism[56], which we excluded because it was a separate disease and did not seem to be relevant to the current study.

Second, Th17 cells are a subset of CD4 + T cells that specifically secrete IL-17, and most Th17-mediated effects involve IL-17 A, which is a key factor in the recruitment, activation and migration of central granulocytes, thereby contributing to inflammation in the anterior segment following alkali burns[51]. This finding was consistent with the results of immunohistochemistry on the 18th day after modeling in this study, which showed that there were many IL-17-positive cells in the corneas from both the radiation-treated UCMSC lens group and the blank lens group, while there were no IL-17-positive cells in the normal corneal tissue. Furthermore, IL-17 has been implicated as a cytokine involved in the pathogenesis of ocular neovascular diseases, including proliferative diabetic retinopathy (PDR), age-related macular degeneration (AMD), retinopathy of prematurity (ROP), and retinal vein occlusion (RVO)[57]. However, proliferation assays revealed that IL-17 does not directly promote the proliferation of human corneal endothelial cells (HCECs), suggesting that IL-17 may function as an indirect angiogenic factor capable of stimulating angiogenesis in vivo[58]. Previous studies have demonstrated that Th17 cells, via IL-17 secretion, upregulate the expression of angiogenic factors such as VEGF and MMPs, thereby driving angiogenesis in both inflammatory and tumor contexts[57,59]. In this study, we observed that co-culture of UCMSCs with peripheral blood mononuclear cells (PBMCs) reduced the proportion of Th17 cells. Notably, the

radiation-treated UCMSC lens group exhibited significantly fewer IL-17-positive cells compared to the blank lens group, indicating that UCMSCs, which are the primary functional component of radiation-treated UCMSC lenses, can effectively inhibit the production and infiltration of Th17 cells. Additionally, we detected reduced expression of VEGF, MMP1, MMP2, and MMP9 in the radiation-treated UCMSC lens group. These findings suggest that the suppression of IL-17 by UCMSCs may be mechanistically linked to the downregulation of these angiogenic factors, ultimately leading to a reduction in corneal neovascularization.

Third, Th17 suppression is associated with multiple secondary pathways and extensive immune regulation, involving complex mechanisms such as cell-cell interactions, signaling pathways, and cytokine networks[60,61]. Th17 cell differentiation mainly includes three stages: induction, expansion and stabilization. At each stage, Th17 cell differentiation is finely and intricately regulated by various cytokines and signaling molecules, and to further examine which stage of the Th17 cell differentiation pathway is the main pathway involved, we tested 10 cytokines from this pathway, not only IL-17, in irradiated UCMSCs on lenses. Among them, radiation-treated UCMSC lenses downregulated the expression of IL-6, which is one of the main factors that promotes Th17 cell differentiation in the induction phase. Moreover, the lenses also downregulated IL-23, which is normally expressed in the stabilization phase, while they upregulated the expression of STAT1, which is involved in inhibiting the induction of Th17 cells induced by IL-6. In addition, radiation-treated UCMSC lenses also reduced the levels of IL-17 A and CCR6, which are products and markers of Th17 cells[62], respectively. In addition, the level of IL-4, which is a negative regulating factor of the differentiation pathway, was significantly increased in the radiation-treated UCMSC lens group, and CD3G, IL-1B, and LAT, which are upregulated in this pathway, were downregulated in the radiation-treated UCMSC lens group compared to the blank lens group. Overall, radiation-treated UCMSCs suppressed the Th17 cell differentiation pathway, especially in the induction phase and the stabilization phase. The evidence above showed that radiation-treated UCMSC lenses successfully inhibited inflammation via inhibition of the Th17 cell differentiation pathway.

This study employed flow cytometry to investigate the correlation between irradiated UCMSC density and Th17 cell frequency. Given the low abundance of CD4 + cells in human PBMCs, CD8-negative selection was used to identify CD4 + T cells, consistent with prior methodologies[63,64]. PBMC-derived T cells comprise three subsets: CD8+/CD4+, CD8+/CD4-, and CD8-/CD4 + T cells[65]. To avoid co-isolating CD8+/CD4 + T cells, a two-step strategy was implemented: CD3 antibody was used to capture total T cells, followed by CD8 antibody to isolate CD8- T cells, enabling efficient CD8-/CD4 + T cell isolation in one step.

We observed that higher UCMSC density enhanced the inhibition of Th17 cell differentiation. Previous studies indicate that UCMSCs secrete immunomodulatory factors such as TGF-β, IL-10, PGE2, and IDO, which are upregulated at higher cellular concentrations. These factors suppress Th17 differentiation by inhibiting STAT3 and RORγt signaling while promoting Treg induction[61,66]. Xu et al. further demonstrated that MSCs inhibit Th17 differentiation via dose-dependent TGF-β secretion[67], suggesting a potential dose-dependent relationship between UCMSC density and Th17 suppression. Further research is needed to elucidate the underlying mechanisms and explore clinical applications.

The limitations of these studies are as follows. First, since the corneal curvature of rabbits is obviously smaller than that of humans, resulting in a poor match between the clinically used bandage lens and the rabbit cornea, and there is a nondegenerate third eyelid, the lenses placed in the rabbit conjunctiva sac may change position due to eye movement, potentially resulting in friction with the cornea, which limits the therapeutic effect on the injured site. For example, among the four experimental groups, the IF scores in the blank lens group were the highest at 3, 7, 10, and 14 days following corneal alkali burn, even exceeding those in the untreated group (Fig. 1). Concurrently, the wound area rate in the blank lens group was the lowest at day 7 but the highest at day 10 post-burn (Fig. 4). This pattern may be attributed to the mechanical friction between the bandage lens and the rabbit cornea, which could have induced corneal damage or even ulcers, leading to the peak IF scores observed in the blank lens group on day 14. On the other hand, the bandage lens also exhibited a protective effect on the cornea, potentially promoting wound healing and reducing corneal inflammation. This may partially explain the observed decrease in IF scores in the blank lens group on day 18 compared to day 14. Second, in this study, the lenses were replaced every 3 to 4 days, as UCMSCs on the lenses maintained high viability and sufficient cell numbers during this period. However, to avoid lenses detaching from the cornea during treatment, the eyelid should be sutured every time, which can affect the experimental results. Third, severe swelling and ulceration of the eyelids on the 18th day led to the relatively short observation time of the rabbit alkali burn model, corneal inflammation in each group of rabbits did not completely subside, and no obvious scar formed, which led to the finding that the effect of UCMSCs on corneal scar formation and inhibition was not recorded in this study. Fourth, there is a lack of therapeutic studies on Th17 cell targets. In further studies, we will complete a Th17 cell differentiation-related gene knockout experiment and observe the therapeutic effect. If the therapeutic effect is significantly decreased, Th17 cell differentiation could be a therapeutic target of UCMSCs for treating corneal alkali burns after radiation.

Conclusions

In general, the efficacy of radiation-treated UCMSC lenses is significantly better than that of blank lenses, especially in terms of their anti-inflammatory effects and inhibition of neovascularization. These lenses can inhibit Th17 cell differentiation and can be easily used by ophthalmologists to treat a variety of ocular surface diseases given their safety and efficacy.

Materials and methods

Acquisition of UCMSCs

Human UC-MSCs were collected upon delivery with informed consent after birth cesarean sections. All experimental procedures were approved by the Ethics Committee of the Third Affiliated Hospital, Sun Yat-sen University. We confirm that all methods were performed in accordance with the relevant guidelines and regulations. According to ICH Q5D, USP, and ISO24603 (the international standard of stem cell), the umbilical cord tissue collection and transportation, UCMSC isolation, and the establishments of a primary cell bank (PCB), a master cell bank (MCB), and a working cell bank (WCB) have been completed, respectively. The UCMSCs from the PCB, MCB, and WCB were comprehensively tested and all results met the established standards. Umbilical cords, which were washed twice with normal saline, were aseptically cut into small pieces and then longitudinally cut. Separated Wharton's jelly samples were cut into small tissue blocks of 1 mm^2, transferred to serum-free medium (Yocon, Beijing, China), and then cultured at 37 °C in 5% CO_2. UCMSCs were selected by flow cytometry (BD Biosciences), and the percentages of cells expressing cluster of differentiation 44 (CD44), CD73, CD90 and CD105 were > 95%, while the percentages of cells expressing CD34 and CD45 were < 5%[68,69]. In addition, UCMSCs were confirmed to differentiate into osteoblasts, adipocytes and chondrogenic cells. UCMSCs that met these criteria were used in subsequent trials.

Preparing lenses with radiation-treated USMSCs

The radiation-treated UCMSC lens preparation has been described in our patent (Patent Number: ZL202011504302.4). Briefly, UCMSCs were digested using TrypLE™ Express (Gibco, Gaithersburg, MD, USA) after they reached 80–90% confluence. UCMSCs were then seeded onto a silicon hydrogel lens for 4 h, and the lens was then irradiated at a dose of 15 Gy, which effectively inhibited UCMSC proliferation but did not affect the levels of anti-inflammatory factors, and we proved that the immune function and activity of the UCMSCs were still present in our previous study[24].

Animals

All animal studies were approved by the Zhongshan Ophthalmic Center Animal Care and Ethics Committee (O2023048) and complied with the Association for Research and Ophthalmology (ARVO) statement on the use of animals in ophthalmic and vision research. All studies were performed in accordance with the ARRIVE guidelines.

Male New Zealand rabbits (3 months old, 2.0–3.0 kg) were purchased from Huadong Xinhua Experimental Animal Nutrition Field (Huadu District, Guangzhou, China). In addition, we confirmed that none of the rabbits had ocular diseases before treatment. After the animal experiment, the rabbits were euthanized by auricular venous injection of overdose of sodium pentobarbital solution.

Rabbit corneal alkali-burn model

Referring to studies by Valeria Villabona-Martinez et al.[70], rabbits were anesthetized by intramuscular injection of 5% (0.1 mL/kg) xylazine hydrochloride and an intravenous injection of 3% (1 mL/kg) pentobarbitone via the ear vein. An 8 mm diameter filter paper disc was dripped with 1 mol/L NaOH solution for 10 s and then placed on the central cornea of the left eye for 30 s. Then, the injured eyes were rinsed with sterile physiological saline (50 mL of 0.9% NaCl) for 1 min.

Grouping and treatments

Part 1: After the burns, twenty rabbits were then randomly divided into four groups ($n = 5$): the untreated group, without lens and intravenous injection of UCMSCs; the blank lens group, treated with blank lenses; the radiation-treated UCMSC lens group, treated with radiation-treated UCMSC lenses (2×10^5 cells per lens); and the UCMSC I.V. group, treated with 15 Gy radiation-treated UCMSCs via intravenous injection (3.47×10^6 cells/kg). The eyelids were immediately closed using three interrupted 6 – 0 sutures (Ethicon; Johnson & Johnson, New Brunswick, NJ, USA). Sutures were removed from all twenty rabbits on days 3, 7, 10, and 14 post-injury. At each time point, corneal characterization was performed using slit lamp imaging and AS-OCT. Subsequently, bandage contact lenses were replaced in the blank lens and radiation-treated UCMSC lens groups, while the UCMSC I.V. group received intravenous injections of UCMSCs (3.47×10^6 cells/kg)[71]. Finally, the eyelids were re-sutured. There was no post-treatment drug regimen after those operations. On day 18, after the slit lamp and AS-OCT examinations, the left eyes were enucleated under deep anesthesia, and the corneas were cut along their diameters and divided into two halves, one half for HE staining and the other half for qRT-PCR. In addition, five normal rabbits (left eyes) were used as the normal control group.

Part 2: Twenty rabbits were then randomly divided into two groups after corneal alkali burns ($n = 10$): the blank lens group and the radiation-treated UCMSC lens group. The treatments were the same as those for the eponymous groups in part 1. After 18 days of treatment, the left eyes were enucleated as part 1, and 2 corneas from each group were examined by transcriptome sequencing, 2 corneas by immunohistochemistry, 3 corneas by qRT-PCR, and 3 corneas by ELISA to determine the therapeutic mechanism of the radiation-treated UCMSC lens. In addition, ten normal rabbits (left eyes) were used as the normal control group.

Slit lamp observation of corneal inflammation

The degree of corneal inflammation was evaluated using the IF, which was recorded by using a slit lamp and was analyzed as previously described[25]. Briefly, the IF was analyzed based on the following parameters: ciliary hyperemia (absent, 0; present but less than 1 mm, 1; present between 1 and 2 mm, 2; present and more than 2 mm, 3; central corneal edema (absent, 0; present with visible iris details, 1; present without visible iris details, 2; present without visible pupil, 3); and peripheral corneal edema (absent, 0; present with visible iris details,

1; present without visible iris details, 2; and present with no visible iris, 3). The final IF result was obtained by summing the results of the different parameters and dividing the sum by a factor of 9. All information was evaluated by the same physician, and this process was repeated twice.

Corneal angiogenesis

On days 3, 7, 10, 14, and 18 after the alkali burn, slit lamp microscopy images of the longest vessel with little continuous curvature and neovascular growth toward the center of the corneal opacity were captured. The corneal neovascular growth area (A) was calculated according to the formula[72]: $A = C/12 \times 3.1416 \times [r^2 - (r-l)]^2$, where C is the number of circumferential clock points of neovascularization involvement in the cornea, l is the length of the neovascularization from the corneal limbus deep into the cornea, and r is the radius of the rabbit cornea, set at a fixed value of 7 mm. All information from the images was evaluated by the same physician, and this process was repeated twice.

Corneal fluorescein staining score

Fluorescein staining of the corneal epithelium was used to evaluate the degree of corneal epithelial damage. Briefly, corneal fluorescein staining was performed before the alkaline burns and at 3, 7, 10, 14, and 18 days after the injury. A 50 μL drop of sodium chloride was injected onto sodium fluorescein ophthalmic paper (Tianjin Jingming New Technological Development Co., Ltd., China), which was subsequently placed on the lower eyelid for staining for 1 min. The corneal staining was observed under a slit lamp microscope with cobalt blue diffuse light. Images of the slit lamp microscope were analyzed and evaluated by the same doctor using ImageJ 1.8.0.172v software (National Institutes of Health, Bethesda, MD). The rate of corneal epithelial damage was calculated as the ratio of the total stained area to the corneal area.

Examination of central corneal thickness using AS-OCT

Referring to the methods used in previous studies[25], rabbits were anesthetized as previously described and then examined using AS-OCT (Heidelberg Engineering, Heidelberg, Germany) at 3, 7, 10, 14 and 18 days after the alkali burn. The results were saved as images and marked to measure the thickness of the central corneas. The scans were obtained using a four-line scanning method, and the corneal thickness was determined by an analysis of the distance from the epithelium to the endothelium. The AS-OCT images were evaluated by the same physician, and the process was repeated twice.

Corneal histological examination

The corneas were fixed with 10% neutral formalin for 24 h and then embedded in paraffin wax. They were continuously sliced at a thickness of 4 μm and dewaxed in water with gradient ethanol-aqueous solution. After deiodination by 5% sodium thiosulfate solution, the sections were successively dyed with hematoxylin and eosin. Optical microscopy (Nikon, Japan) was performed at 100× and 200×. All examinations and assessments were performed by the same doctor.

RNA extraction and sequencing

RNA extraction was performed using TRIzol™ (Invitrogen, 15596026) and Direct-zol™ RNA Miniprep (ZYMO Research, R2050). Sequencing libraries were generated using the SEQUMED® MustSeq® 3'mRNA DEG kit (Sequmed, China). The library preparations were sequenced on the Illumina NovaSeq 6000 S4 platform. Reads were aligned to the reference genome using HISAT2, and reference genome and gene model annotation files were downloaded from Ensembl. Gene expression level quantification was performed using featureCounts. Genes with a p value < 0.05 and |fold change| > 2 according to DESeq2 were considered differentially expressed. Kyoto Encyclopedia of Genes and Genomes (KEGG) enrichment analysis and gene set enrichment analysis (GSEA) were performed with clusterProfiler.

Relationship between irradiated UCMSC density and Th17 cell numbers

UCMSCs were seeded in six-well plates and divided into two experimental groups: the low-density group (9.0×10^4 cells/well) and the high-density group (9.0×10^5 cells/well). All UCMSCs were irradiated with 15 Gy and treated with mitomycin C for 20 min the following day to inhibit proliferation. Subsequently, peripheral blood mononuclear cells (PBMCs, 1×10^6 cells/well) were added to the six-well plates, with a trans-well system used to separate the two cell types. Control group A served as a blank control, while control group B consisted of PBMCs (1×10^6 cells) cultured alone. After 48 h of co-culture in the experimental groups, a leukocyte activation cocktail containing BD GolgiPlug was added to each well. Cells were harvested after an additional 5 hours of culture.

After centrifugation, the cells were divided into 5 tubes (tubes A ~ E). The cells in tube A were incubated with a CD3 antibody (1:500, ab16669, Abcam, Cambridge, UK) for 30 min followed by incubation with goat anti-rabbit IgG H&L (Alexa Fluor® 488) (ab150077, Abcam, Cambridge, UK) against CD3 primary antibody; those in tube B were incubated with a CD8 antibody (1:500, ab60076, Abcam, Cambridge, UK) for 30 min followed by incubation with goat anti-rat IgG H&L (PE) (ab7010, Abcam, Cambridge, UK) against CD8 primary antibody; those in tube C were incubated with an IL-17 antibody (1:100, ab79056, Abcam, Cambridge, UK) for 30 min followed by incubation with goat anti-rabbit IgG (H&L) (Alexa Fluor™ Plus 647), (Thermo Fisher Scientific, A32733, USA) after fixation with 4% paraformaldehyde for 30 min and permeation with 1% Triton X-100 for 15 min; those in tube D were incubated with an IL-17 antibody for 30 min after incubation with CD3 and CD8 antibodies for 30 min, fixation with 4% paraformaldehyde for 30 min, and permeation with 1% Triton X-100 for 15 min; and those in tube E were used as a blank control. All of the cells were analyzed by flow cytometry (Sparrow, Celula, Chengdu, CN), and the proportions of Th17 cells were recorded. The proliferation inhibition

Genes	Forward sequences	Reverse sequences
rab -VEGF	AGGAGACAATAAACCCCACG	TGATCTGCATGGTGACGTTGA
rab -INF-γ	CCTTTCTGTGCTGTCGATGGG	GAACCCAAGATGAGGCAGAGC
rab -IL-4	GCGACATCATCCTACCCGAA	TCGGTTGTGTTCTTGGGGAC
rab -IL-23	TCCGCTTCAAGATCCTTCGC	TTAGGGGCTCAGAGTTGCCG
rab -MMP-1	CCATTCCCTTGGACTCTCCCA	GGGCCTACTGGCTGACTGG
rab -MMP-2	ACCCGGATGTGGCCAACTATA	TATCCGTCTCCATGCTCCCAG
rab- MMP-9	GCCTTTGAACACACACGACG	GGGTACTCACACGCCAGAAG
rab -CD3G	GGCAGGTGTTCTCCATTCCAT	CGATAGGTGGCGCTCTCAAAA
rab -LAT	AGAAAGGTCCGTGTGTGGTTG	ACGGAGATTATTCGAGCCCCA
rab -STAT1	GTGATCTCCAACGTCAGCCAG	CCGGCATTAGGACCAAGTAGC
rab -IL-1B	GTCGTTGTGGCTCTGGAGAAG	GCTCATACGTGCCAGACAACA
rab -IL-6	GAATCACTTCGGGGCTGATGG	GCTTGAGGGTGGCTTCTTCAT
rab -CCR6	CGTGTACCTCCTGAACATGGC	TCCCGCAGTTGAAGTTGATGG
rab -IL-17 A	AATGCCGCGAAATCCAGGATG	TGGTCCTCATTCCCTTCAGCA

Table 1. Primer sequences.

rate of Th17 cells was calculated using the following formula: proliferation inhibition rate = [1 - (experimental group - control group A)/(control group B - control group A)] × 100%.

Immunohistochemistry

After the corneas were collected from the blank lens group and the radiation-treated UCMSC lens group, they were fixed in 10% neutral formalin for 24 h, and the samples were embedded in paraffin, serially sectioned at a thickness of 4 μm and rehydrated with graded ethanol–water solutions. Endogenous peroxidase activity was blocked by incubating the sections with 30 mL/L hydrogen peroxidase for 25 min. The sections were incubated overnight at 4 °C with a guinea pig anti-rabbit IL-17 antibody (1:100, Abcam PLC, Cambridge, UK), and a goat anti-guinea pig IgG antibody (1:500, Biomatik, Kitchener, Ontario, N2C 1N6, Canada) was used as the secondary antibody. The slides were incubated with diaminobenzidine and counterstained with hematoxylin. IL-17 cells appeared brown after staining. Next, the sections were analyzed using standard light microscopy (Nikon, Japan) at 200× and 400× magnification. Two observers blindly assessed the images of all the samples.

ELISA

The corneal tissues collected from the blank lens group and the radiation-treated UCMSC lens group were washed in precooled phosphate buffer (pH 7.0-7.2) to remove blood, cut into pieces after weighing, added to a glass homogenizer with the corresponding volume of phosphate buffer (volume ratio of 1:9), and fully ground on ice. Finally, the prepared homogenate was centrifuged for 10 min, and the supernatant was taken as the sample.

After the Rabbit IL-17 ELISA Kit (ELK Biotechnology Co., Ltd., Wuhan, Hubei, China) and samples were equilibrated at room temperature, standard diluent buffer (100 μL) or sample diluent buffer (100 μL) was added to precoated microplates and incubated at 37 °C for 80 min. After the liquid in the enzyme label plate was discarded, 200 μL of washing buffer was added to each well, and the plates were washed 3 times. Then, 100 μL of biotinylated antibody was added to each well, and the plates were incubated at 37 °C for 50 min. After the liquid was discarded and the plate was washed, 100 μL of streptavidin-horseradish peroxidase (HRP) working solution was added to each well, and the plate was incubated at 37 °C for 50 min. After repeated washing, 90 μL of 3,3',5,5'-tetramethylbenzidine (TMB) substrate solution was added to each well and incubated at 37 °C for 20 min. Finally, 50 μL of stop reagent was added to each well, and the plate was immediately read at 450 nm in an ELISA plate reader (Molecular Devices, USA) to obtain the results.

qRT–PCR

The master mix was prepared in an RNase-free centrifuge tube. The input amount of RNA was 600 ng. A total of 1 μL of gDNA digester, 2 μL of 5× gDNA digester buffer, and RNase-free ddH_2O were added (total volume of 10 μL) and then gently mixed, followed by incubation at 42 °C for 2 min. Then, 10 μL of 2 × 1st Strand cDNA Syn-thesis SuperMix for qPCR (Hifair™, Yeason, Shanghai, China) was directly added to the above reaction tube and gently mixed using a pipette. This mixture was incubated at 25 °C for 5 min, 42 °C for 30 min, and 85 °C for 5 min. The reaction system was prepared in an RNase-free centrifuge tube with 600 ng of cDNA input, 10 μL of Hieff qPCR SYBR Green Master Mix, 0.4 μL of forward primer, 0.4 μL of reverse primer, and sterile ultrapure water to make up the system to 20 μL, followed by gentle mixing using a pipette. The abovementioned mixture was incubated at 95 °C for 5 min (95 °C for 10 s and 60 °C for 30 s) for 40 cycles. The primer sequences are listed in Table 1.

Statistical analysis

Prism 9 software (GraphPad, San Diego, CA, USA) was used to perform the statistical analysis. Data comparison between two groups was conducted by the two-tailed unpaired Student's t test, and data comparison among

multiple groups was carried out by one-way analysis of variance (ANOVA). All the data are expressed as the mean ± standard deviation. A value of $P < 0.05$ was considered to indicate statistical significance.

Data availability

The authors confirm that the data supporting the findings of this study are available within the article.

Received: 29 September 2024; Accepted: 18 March 2025
Published online: 26 March 2025

References

1. Bakunowicz-Łazarczyk, A. & Urban, B. Assessment of therapeutic options for reducing alkali burn-induced corneal neovascularization and inflammation. *Adv. Med. Sci.* **61**, 101–112 (2016).
2. Torres, J. et al. Torsional wave elastography to assess the mechanical properties of the cornea. *Sci. Rep.* **12**, 8354 (2022).
3. Almaliotis, D. et al. Mesenchymal stem cells improve healing of the cornea after alkali injury. *Graefes Arch. Clin. Exp. Ophthalmol.* **253**, 1121–1135 (2015).
4. 4 Kethiri, A. R. et al. Long term observation of ocular surface alkali burn in rabbit models: quantitative analysis of corneal haze, vascularity and self-recovery. *Exp. Eye Res.* **205**, 108526 (2021).
5. Poon, A. C. et al. Autologous serum Eyedrops for dry eyes and epithelial defects: clinical and in vitro toxicity studies. *Br. J. Ophthalmol.* **85**, 1188–1197 (2001).
6. Baylis, O. et al. 13 Years of cultured limbal epithelial cell therapy: a review of the outcomes. *J. Cell. Biochem.* **112**, 993–1002 (2011).
7. Brodovsky, S. C. et al. Management of alkali Burns: an 11-year retrospective review. *Ophthalmology* **107**, 1829–1835 (2000).
8. Mittal, S. K. et al. Restoration of corneal transparency by mesenchymal stem cells. *Stem Cell. Rep.* **7**, 583–590 (2016).
9. Kharod-Dholakia, B. et al. Prevention and treatment of corneal graft rejection: current practice patterns of the cornea society. *Cornea* **34**, 609–614 (2011).
10. Dumitru, C. A. et al. Stimulation of mesenchymal stromal cells (MSCs) via TLR3 reveals a novel mechanism of autocrine priming. *FASEB J.* **28**, 3856–3866 (2014).
11. Yao, L. et al. Role of mesenchymal stem cells on cornea wound healing induced by acute alkali burn. *PLoS One.* **7**, e30842 (2012).
12. Shukla, S. et al. Therapeutic efficacy of different routes of mesenchymal stem cell administration in corneal injury. *Ocul Surf.* **17**, 729–736 (2019).
13. Di, G. H. et al. Therapeutic effect of secretome from TNF-alpha stimulated mesenchymal stem cells in an experimental model of corneal limbal stem cell deficiency. *Int. J. Ophthalmol.* **14**, 179–185 (2021).
14. Tao, H. et al. Mesenchymal stem Cell-Derived extracellular vesicles for corneal wound repair. *Stem Cells Int.* **2019**, 5738510 (2019).
15. Ma, Y. et al. Reconstruction of chemically burned rat corneal surface by bone marrow-derived human mesenchymal stem cells. *Stem Cells.* **24**, 315–321 (2006).
16. 16 Shukla, S. et al. Therapeutic efficacy of different routes of mesenchymal stem cell administration in corneal injury. *Ocul Surf.* **17**, 729–736 (2019).
17. Tan, Y., Ooi, S. & Wang, L. Immunogenicity and tumorigenicity of pluripotent stem cells and their derivatives: genetic and epigenetic perspectives. *Curr. Stem Cell. Res. Ther.* **9**, 63–72 (2014).
18. Huldani, H. et al. Application of extracellular vesicles derived from mesenchymal stem cells as potential therapeutic tools in autoimmune and rheumatic diseases. *Int. Immunopharmacol.* **106**, 108634 (2022).
19. Liu, M. et al. Mesenchymal stem cells from bone marrow show a stronger stimulating effect on megakaryocyte progenitor expansion than those from non-hematopoietic tissues. *Platelets* **21**, 199–210 (2010).
20. Bengani, L. C. et al. Contact lenses as a platform for ocular drug delivery. *Expert Opin. Drug Deliv.* **10**, 1483–1496 (2013).
21. Agrahari, V. et al. A comprehensive insight on ocular pharmacokinetics. *Drug Deliv Transl Res.* **6**, 735–754 (2016).
22. Riau, A. K. et al. Sustained delivery system for stem Cell-Derived exosomes. *Front. Pharmacol.* **10**, 1368 (2019).
23. 23 Ghazaryan, E. et al. Mesenchymal stem cells in corneal neovascularization: comparison of different application routes. *Mol. Med. Rep.* **14**, 3104–3112 (2016).
24. Liu, Y. et al. MSCohi-O lenses for long-term retention of mesenchymal stem cells on ocular surface as a therapeutic approach for chronic ocular graft-versus-host disease. *Stem Cell. Rep.* **18**, 2356–2369 (2023).
25. Wang, T. et al. Evaluation of the effects of Biohcly in an in vivo model of mechanical wounds in the rabbit cornea. *J. Ocul Pharmacol. Ther.* **35**, 189–199 (2019).
26. Ling, S. et al. Clinical and experimental research of corneal lymphangiogenesis after keratoplasty. *Ophthalmologica* **222**, 308–316 (2008).
27. Zhang, Z. et al. Plasminogen kringle 5 inhibits alkali-burn-induced corneal neovascularization. *Invest. Ophthalmol. Vis. Sci.* **46**, 4062–4071 (2005).
28. Laria, C., Alió, J. L. & Ruiz-Moreno, J. M. Combined non-steroidal therapy in experimental corneal injury. *Ophthalmic Res.* **29**, 145–153 (1997).
29. 29 Shibuya, M. Vascular endothelial growth factor (VEGF) and its receptor (VEGFR) signaling in angiogenesis: A crucial target for anti- and pro-angiogenic therapies. *Genes Cancer.* **2**, 1097–1105 (2011).
30. 30 Kessenbrock, K., Plaks, V. & Werb, Z. Matrix metalloproteinases: regulators of the tumor microenvironment. *Cell* **141**, 52–67 (2010).
31. 31 Zhang, J. Regulation of matrix metalloproteinases 2 and 9 in corneal neovascularization. *Chem. Biol. Drug Des.* **95**, 485–492 (2020).
32. McGeachy, M. J. & Cua, D. J. Th17 cell differentiation: the long and winding road. *Immunity* **28**, 445–453 (2008).
33. Gu, H. W. et al. Effects of amniotic membrane transplantation on cytokines expression in chemically burned rat Corneas. *Int. J. Ophthalmol.* **4**, 33–36 (2011).
34. Hirahara, K. et al. Signal transduction pathways and transcriptional regulation in Th17 cell differentiation. *Cytokine Growth Factor. Rev.* **21**, 425–434 (2010).
35. Singh, S. P. et al. Human T cells that are able to produce IL-17 express the chemokine receptor CCR6. *J Immunol.* **180**, 214–221 (2008).
36. Markegard, E. et al. Basal LAT-diacylglycerol-RasGRP1 signals in T cells maintain TCRα gene expression. *PLoS One* **6**, e25540 (2011).
37. Zhu, Y. et al. Lowering glycosphingolipid levels in CD4 + T cells attenuates T cell receptor signaling, cytokine production, and differentiation to the Th17 lineage. *J. Biol. Chem.* **286**, 14787–14794 (2011).
38. Li, G. et al. Human limbal niche cells are a powerful regenerative source for the prevention of limbal stem cell deficiency in a rabbit model. *Sci. Rep.* **8**, 6566 (2018).
39. Dinc, E. et al. Evaluation of Anti-Inflammatory and antiapoptotic effects of bone marrow and Adipose-Derived mesenchymal stem cells in acute alkaline corneal burn. *J. Ocul Pharmacol. Ther.* **37**, 24–34 (2021).

40. Ye, J., Yao, K. & Kim, J. C. Mesenchymal stem cell transplantation in a rabbit corneal alkali burn model: engraftment and involvement in wound healing. *Eye (Lond.)* **20**, 482–490 (2006).
41. Melzer, C., von der Ohe, J. & Hass, R. MSC stimulate ovarian tumor growth during intercellular communication but reduce tumorigenicity after fusion with ovarian cancer cells. *Cell. Commun. Signal.* **16**, 67 (2018).
42. Xue, J. et al. Tumorigenic hybrids between mesenchymal stem cells and gastric cancer cells enhanced cancer proliferation, migration and stemness. *BMC Cancer*. **15**, 793 (2015).
43. Li, Q. et al. Effects of human umbilical cord-derived mesenchymal stem cells on hematologic malignancies. *Oncol. Lett.* **15**, 6982–6990 (2018).
44. Meshitsuka, S. et al. CRISPR/Cas9 and AAV mediated insertion of B2 microglobulin-HLA-G fusion gene protects mesenchymal stromal cells from allogeneic rejection and potentiates the use for off-the-shelf cell therapy. *Regen Ther.* **21**, 442–452 (2022).
45. Zhang, M. et al. SDF-1 expression by mesenchymal stem cells results in trophic support of cardiac myocytes after myocardial infarction. *FASEB J.* **21**, 3197–3207 (2007).
46. Barbash, I. M. et al. Systemic delivery of bone marrow-derived mesenchymal stem cells to the infarcted myocardium: feasibility, cell migration, and body distribution. *Circulation* **108**, 863–868 (2003).
47. Roddy, G. W. et al. Action at a distance: systemically administered adult stem/progenitor cells (MSCs) reduce inflammatory damage to the cornea without engraftment and primarily by secretion of TNF-α stimulated gene/protein 6. *Stem Cells* **29**, 1572–1579 (2011).
48. Oh, J. Y. et al. The anti-inflammatory and anti-angiogenic role of mesenchymal stem cells in corneal wound healing following chemical injury. *Stem Cells* **26**, 1047–1055 (2008).
49. Sohni, A. & Verfaillie, C. M. Mesenchymal stem cells migration homing and tracking. *Stem Cells Int.* **2013**, 130763 (2013).
50. Yang, S. J. et al. Ectopic vascularized bone formation by human umbilical cord-derived mesenchymal stromal cells expressing bone morphogenetic factor-2 and endothelial cells. *Biochem. Biophys. Res. Commun.* **504**, 302–308 (2018).
51. González, P. L. et al. Chorion mesenchymal stem cells show superior differentiation, immunosuppressive, and angiogenic potentials in comparison with haploidentical maternal placental cells. *Stem Cells Transl Med.* **4**, 1109–1121 (2015).
52. Hertsenberg, A. J. et al. Corneal stromal stem cells reduce corneal scarring by mediating neutrophil infiltration after wounding. *PLoS One*. **12**, e0171712 (2017).
53. Jiang, T. S. et al. Reconstruction of the corneal epithelium with induced marrow mesenchymal stem cells in rats. *Mol. Vis.* **16**, 1304–1316 (2010).
54. Chung, E. et al. Fibrin-based 3D matrices induce angiogenic behavior of adipose-derived stem cells. *Acta Biomater.* **17**, 78–88 (2015).
55. Ueta, M. et al. Immunosuppressive properties of human amniotic membrane for mixed lymphocyte reaction. *Clin. Exp. Immunol.* **129**, 464–470 (2002).
56. Li, W., Huang, E. & Gao, S. Type 1 diabetes mellitus and cognitive impairments: A systematic review. *J. Alzheimers Dis.* **57**, 29–36 (2017).
57. 57 Li, Y. & Zhou, Y. Interleukin-17: the role for pathological angiogenesis in ocular neovascular diseases. *Tohoku J. Exp. Med.* **Feb; 247**, 87–98 (2019).
58. 58 Chen, Y. et al. Interleukin-17 induces angiogenesis in human choroidal endothelial cells in vitro. *Invest. Ophthalmol. Vis. Sci.* **55**, 6968–6975 (2014).
59. Shibabaw, T., Teferi, B. & Ayelign, B. The role of Th-17 cells and IL-17 in the metastatic spread of breast cancer: as a means of prognosis and therapeutic target. *Front. Immunol.* **14**, 1094823 (2023).
60. Littman, D. R. & Rudensky, A. Y. Th17 and regulatory T cells in mediating and restraining inflammation. *Cell* **140**, 845–858 (2010).
61. Ivanov, I. I. et al. The orphan nuclear receptor RORgammat directs the differentiation program of Proinflammatory IL-17 + T helper cells. *Cell*ì **126**, 1121–1133.
62. Petrou, P. et al. Safety and clinical effects of mesenchymal stem cells secreting neurotrophic factor transplantation in patients with amyotrophic lateral sclerosis: results of phase 1/2 and 2a clinical trials. *JAMA Neurol.* **73**, 337–344 (2016).
63. 63 Gu, C. et al. Kurarinone regulates Th17/Treg balance and ameliorates autoimmune uveitis via Rac1 Inhibition. *J. Adv. Res.* **24:S2090-1232** (24), 00113–00119 (2024).
64. 64 Liu, X. et al. Insights gained from single-cell analysis of immune cells in Tofacitinib treatment of Vogt-Koyanagi-Harada disease. *JCI Insight*. **7** (23), e162335 (2022).
65. Steier, Z. et al. The CD4 versus CD8 T cell fate decision: A Multiomics- informed perspective. *Annu. Rev. Immunol.* **42**, 235–258 (2024).
66. Soleymaninejadian, E., Pramanik, K. & Samadian, E. Immunomodulatory properties of mesenchymal stem cells: cytokines and factors. *Am. J. Reprod. Immunol.* **67**, 1–8 (2012).
67. Xu, K. et al. Human umbilical cord mesenchymal stem cell-derived small extracellular vesicles ameliorate collagen-induced arthritis via Immunomodulatory T lymphocytes. *Mol. Immunol.* **135**, 36–44 (2021).
68. Wang, J. et al. Manufacture and quality control of human umbilical Cord-Derived mesenchymal stem cell sheets for clinical use. *Cells* **11**, 2732 (2022).
69. Van Pham, P. et al. Isolation and proliferation of umbilical cord tissue derived mesenchymal stem cells for clinical applications. *Cell. Tissue Bank.* **17**, 289–302 (2016).
70. Villabona-Martinez, V. et al. Standardization of corneal alkali burn methodology in rabbits. *Exp. Eye Res.* **230**, 109443 (2023).
71. Sun, H. et al. Promoting effect and mechanism of bone marrow mesenchymal stem cell injection on corneal repair in alkali burn rabbits. *Shandong Med. J.* **57**, 40–42 (2017).
72. Kato, T. et al. Diminished corneal angiogenesis in gelatinase A-deficient mice. *FEBS Lett.* **508**, 187–190 (2001).

Acknowledgements

We are thankful for the equipment support provided by the State Key Laboratory of Ophthalmology, Zhongshan Ophthalmic Center and Guangdong Procapzoom Biosciences Co., Ltd.

Author contributions

S.L. conceptualized the article design, supervised the experiments, and guided the writing of the manuscript. S. S. wrote the manuscript. S.S., Y.C., W.L., H.Y., and Z.L. conducted the animal experiments, collected the data and performed the data analyses. M.L., J.L., Q.H., and Y.L. validated the results. S.S. and Y.C. guided the in vitro experiments. S.L. guided the overall experimental design and helped revise the manuscript.

Funding

This work was supported by the Guangzhou Huangpu International Science and Technology Collaboration Project [grant number 2021GH08].

Declarations

Competing interests
The authors declare no competing interests.

Additional information
Correspondence and requests for materials should be addressed to S.L.

Reprints and permissions information is available at www.nature.com/reprints.

Publisher's note Springer Nature remains neutral with regard to jurisdictional claims in published maps and institutional affiliations.